## PAPER

Check for updates

# Computational study on the mechanisms and kinetics of the CH₂BrO₂ + ClO reaction in the atmosphere†

Yunju Zhang, [iD] *[a] Yizhen Tang[b] and Bing He[c]

The singlet and triplet potential energy surfaces for the $CH_2BrO_2$ + ClO reaction are studied at the CCSD(T)/cc-pVTZ//B3LYP/6-311++G(d,p) level. $CH_2BrO_2$ is revealed to react with ClO through two kinds of mechanisms on the triplet potential energy surface (PES), namely, $S_N2$ displacement and H-abstraction, and the production of P3 ($CHBrO_2$ + HOCl) via H-abstraction is the dominant channel. Addition/elimination and $S_N2$ displacement mechanisms exist on the singlet PES and are more complicated. The RRKM calculations of the mechanism and product distribution in the $CH_2BrO_2$ + ClO reaction show that the stabilization of IM1 ($CH_2BrOOOBr$) is dominant at $T \leq 600$ K, while the pathway of producing P1 ($CHBrO + HO_2 + Cl$) occupies the entire reaction at $T > 600$ K. The total rate constants are independent of pressure, while the individual rate constants are sensitive to pressure. The lifetime of $CH_2BrO_2$ in the presence of ClO is estimated to be 20.27 h. Moreover, time-dependent density functional theory (TDDFT) calculations suggest that IM1 ($CH_2BrOOOCl$), IM2 ($CH_2BrOOClO$) and IM3 ($CH_2BrOClO_2$) will photolyze under the sunlight.

## 1. Introduction

Owing to the significant contribution of halogens to stratospheric ozone depletion, the atmospheric oxidation of halogens has been extensively studied in the past decades. In recent years, the oxidation process of halogenated compounds was investigated in the atmosphere because these compounds are conducive to the conversion of halogens in the stratosphere.[1,2] Significant attention has been focused on chlorine compounds, which have a huge impact on the atmosphere. Although the concentration of bromine is very low, it can deplete the stratospheric ozone very effectively; thus, it plays an important role in stratospheric chemistry.[3,4] The oxidation process of brominated compounds has aroused the interest of researchers in recent years. The $CH_2Br$ radical is obtained either by $CH_3Br$ reacting with OH/Cl, which abstracts an H atom from $CH_3Br$, or the photolysis of C–Br bonds in $CH_2Br_2$; the $CH_2Br$ radical further reacts with ambient $O_2$ to produce $CH_2BrO_2$:[5]

$$CH_3Br + OH/Cl \rightarrow CH_2Br + H_2O/HCl$$

$$CH_2Br \xrightarrow{h\nu} CH_2Br + Br$$

$$CH_2Br + O_2 \rightarrow CH_2BrO_2$$
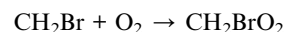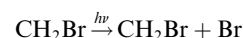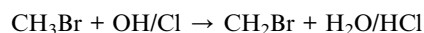
Because of the significant role of halogens in the stratosphere and troposphere, more and more attention has been focused on them in recent years. For instance, the reactions of ClO with the organic peroxy radicals such as $HO_2$, $CH_3O_2$, $CF_3O_2$, $CFCl_2O_2$ $CFCl_2CH_2O_2$ and $CH_3CFClO_2$ have been reported experimentally and theoretically.[6–16] However, no studies have been reported for the $CH_2BrO_2$ + ClO reaction that, in principle, may contribute to the removal of $CH_2BrO_2$ and ClO and thereby impact stratospheric ozone depletion. Therefore, we first reported the mechanisms of $CH_2BrO_2$ + ClO, and the possible product channels are presented in Scheme 1. The present theoretical study aims at providing a description of the mechanism and kinetics of the multiple channel reaction and supply data about the gas phase reaction of $CH_2BrO_2$ + ClO by employing high-level quantum chemical methods and RRKM-TST theory,[17] which has been successfully used with complex reactions.[18–23] In the present kinetic calculations, we used a modified computer program written for the $C_2H_5CO$ + $O_2$ reaction by Hou and Wang.[19]

[a]Key Laboratory of Photoinduced Functional Materials, Mianyang Normal University, Mianyang 621000, PR China. E-mail: zhangyj010@nenu.edu.cn; Fax: +86 816 2200819; Tel: +86 816 2200064

[b]School of Environmental and Municipal Engineering, Qingdao University of Technology, Fushun Road 11, Qingdao, Shandong, 266033, P. R. China

[c]College of Chemistry and Life Science, Institute of Functional Molecules, Chengdu Normal University, Chengdu, Sichuan 611130, PR China

† Electronic supplementary information (ESI) available. See DOI: 10.1039/c9ra10511e

**Scheme 1** The reaction pathways of the $CH_2BrO_2$ + ClO reaction on the singlet and triplet PESs.

## 2. Computational methods

### 2.1 Electronic structure calculations

Full geometry optimizations (including reactants, intermediates, transition states and products) were carried out at the B3LYP[24,25] level of theory using the 6-311++G(d,p) basis set. The B3LYP method has been proven to be an economical and accurate computational model for predicting electronic structures and has been employed widely.[26,27] Compared with other levels of theory, it was found to be sufficiently accurate for predicting the reliable geometries of the stationary points. At the same time, it is not expensive computationally for scanning the potential energy surface. Moreover, B3LYP theory can effectively suppress the problem of spin contaminants. At the same level of geometry optimization, all stationary points were characterized by harmonic vibrational frequency analysis (the number of imaginary frequencies, NIMAG, 0 for minima and 1 for transition state). To confirm that a transition state connects the right reactants and products, the intrinsic reaction coordinate (IRC)[28,29] path was performed at the B3LYP/6-311++G(d,p) level of theory. Based on the B3LYP/6-311++G(d,p) level optimized geometries, the single-point energies of all the species were refined by coupled cluster theory with single and double with perturbative triple excitations CCSD(T)[30] with the cc-pVTZ basis set. To ensure that all stationary points were treated with a single-reference based wave function, the $T_1$-diagnostic was evaluated for each point using CCSD(T)/cc-pVTZ. The $T_1$ diagnostic value gives a qualitative assessment of the significance of non-dynamic correction. For closed-shell systems, values exceeding 0.02 are suspect. However, Lee et al.[31] suggested that $T_1$-diagnostic values for open-shell systems may be larger. A number of studies have shown that the multireference wave function is significant if the $T_1$ diagnostic value calculated

is greater than 0.045.[31-34] The $T_1$ values of the closed-shell and open-shell species in our system are smaller than 0.02 and 0.045, except for TS6, TS13, TS14, T-TS2, and T-TS4. Fortunately, the five species are not important on the triplet and singlet potential energy surfaces and do not affect the reaction mechanism and dynamic behavior. All the calculations were carried out using the GAUSSIAN 09 program package.[35]

### 2.2 Calculations of rate constants

The microcanonical rate constant was calculated using the RRKM theory as follows:

$$k_i(E) = \alpha_i C_i N_i(E_i^{\neq})/h\rho_j(E_j)$$

In the above equation, $\alpha_i$ is the statistical factor (degeneracy) for the $i$th reaction path. $N_i(E_i^{\neq})$ is the number of states at the energy above the barrier height for transition state $i$; $\rho_j(E_j)$ is the density of states at energy $E_j$ of the intermediate. The density of states and the number of states were calculated using the extended Beyer–Swinehart algorithm.[36,37]

## 3. Results and discussion

The corresponding equilibrium structures of the intermediates and transition states are depicted in Fig. 1, and all the reactants and products are depicted in Fig. 2, with the corresponding limited experimental data.[38] The computational bond lengths of $CH_2O$, $OClO$, $HOCl$, $HO_2$, $ClO$, $HCl$, $O_2(^3\Sigma)$ and $O_3$ are in good agreement with the corresponding experimental values. To clarify the reaction mechanism, the relevant pathways of the singlet and triplet PESs for the $CHBr_2O_2$ + ClO reaction at the CCSD(T)/cc-pVTZ//B3LYP/6-311++G(d,p) level are depicted in Fig. 3. Table S1† summarizes the
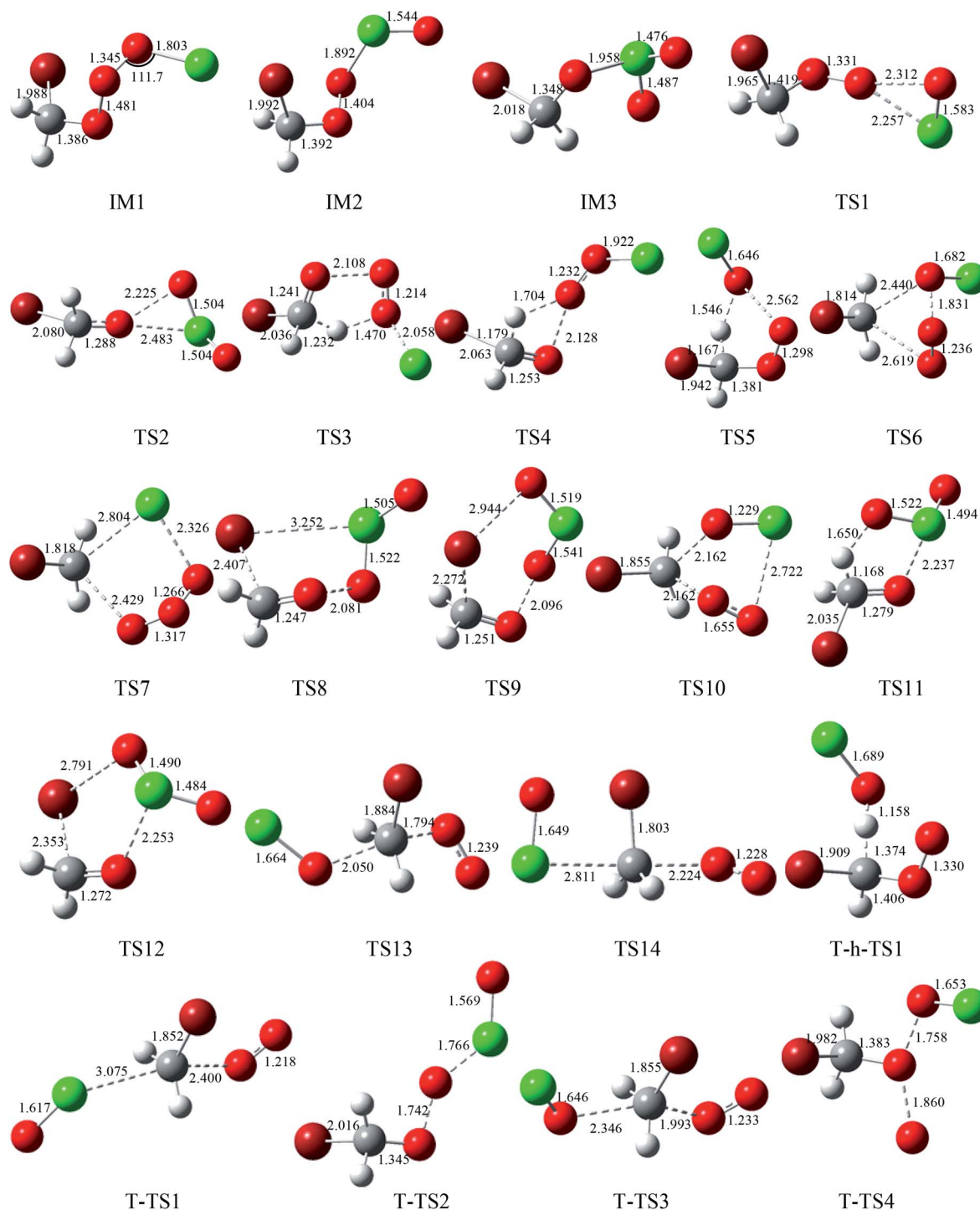
Fig. 1 Optimized geometries (length in Å and angle in degree) for all the intermediates and transition states at the B3LYP/6-311++G(d,p) level.

relative energies including the ZPE corrections of the stationary points. The Z-matrix Cartesian coordinates of all species found on the singlet and triplet PESs are shown in Table S2.† Table S3† displays the harmonic vibrational frequencies and the moment of inertia of all the intermediate and transition states along with available experimental values.

For the title reaction, our results indicate that addition/ elimination and $S_N2$ displacement mechanisms take place on

the singlet PES, while $S_N2$ displacement and H-abstraction mechanisms occur on the triplet PES. Next, we will provide a detailed discussion of these processes.

### 3.1 The mechanism on the singlet PES

**3.1.1 The production of adducts on the singlet PES.** On the singlet surface, the most significant characteristic of the
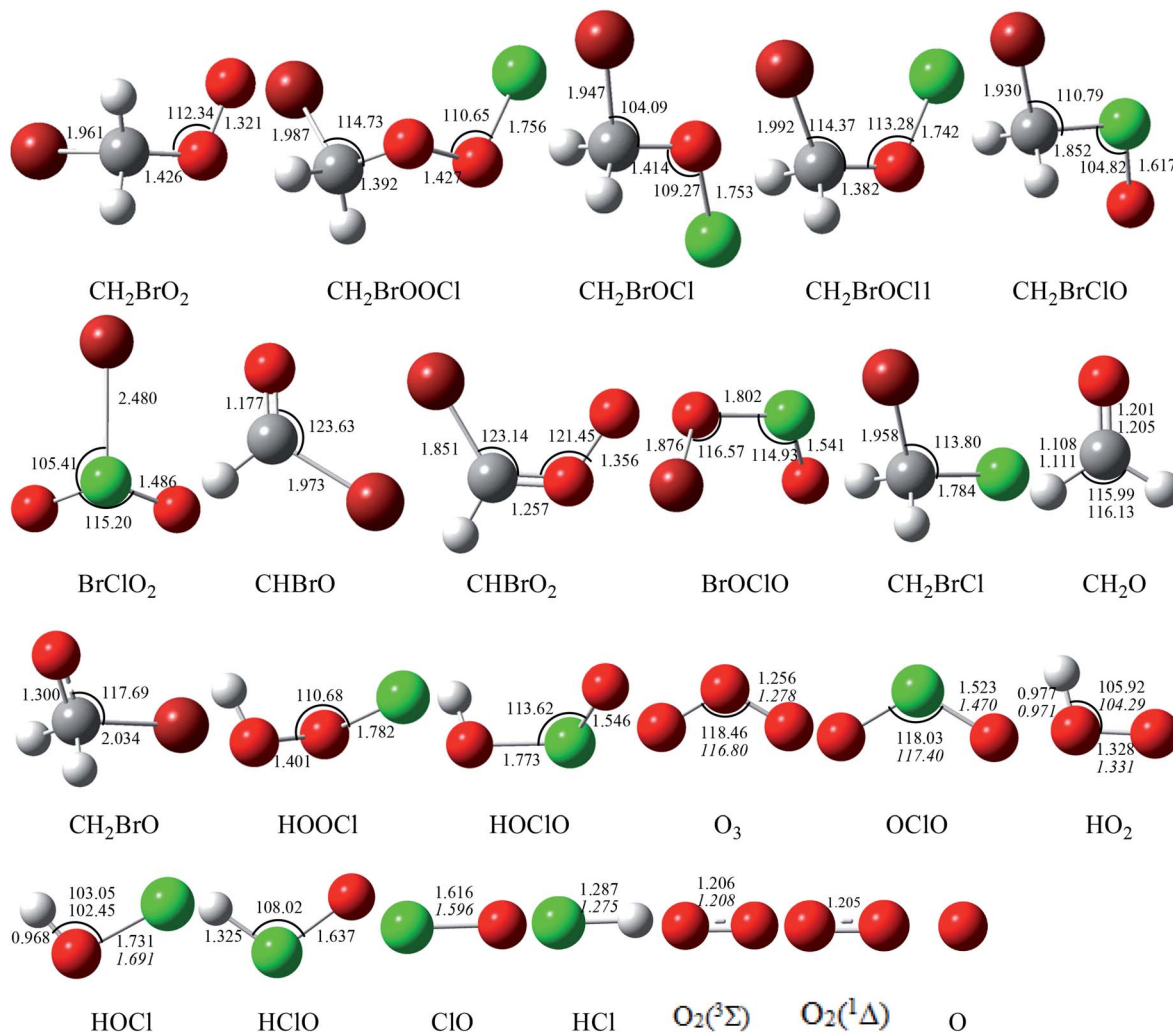
Fig. 2 Optimized geometries (length in Å and angle in degree) for all the reactants and products at the B3LYP/6-311++G(d,p) level. The values in italics are experimental data from ref. 38.

potential energy surface (PES) of the CH₂BrO₂ + ClO reaction is the ability to form the minimum peroxide compound IM1 (CH₂BrOOOCl) with no barrier. The newly formed O–O bond is 1.345 Å, the other O–O and C–Br bonds are somewhat longer, and the C–O bond is somewhat smaller than those in the CH₂BrO₂ radical. The isomer IM2 (CH₂BrOOClO) is more unstable than IM1 (CH₂BrOOOCl) and may be formed passing through the isomerization transition state TS1. TS1 presents a OOCl three-center geometry, which is formed by migration of the Cl atom to the middle-O atom, accompanied with cleavage of the O–O bond. The migrating chlorine is found 2.257 Å away from the shifting end-O by decreasing the OOCl angle from 111.7° to 68.9° and the breaking O–O bond is 2.312 Å. The barrier for IM1 (CH₂BrOOOCl) → TS1 → IM2 (CH₂BrOOClO) is 28.2 kcal mol⁻¹, and IM2 (CH₂BrOOClO) is still 2.2 kcal mol⁻¹ higher than the separate molecular CH₂BrO₂ + ClO, so the isomerization process may be possible at high temperatures. Subsequently, IM2 (CH₂BrOOClO) can surmount the TS2 barrier, leading to IM3 (CH₂BrOClO₂), where the –ClO is transferred to the middle-O atom of the COO– skeleton, and the

simultaneous breakage of the O–O bond occurs. The O–O bond breaking in the triangular TS2 is stretched to 2.225 Å and the formed Cl–O bond is 2.483 Å long. The magnitude of the imaginary frequency for TS2 is 140i cm⁻¹. The barrier for the IM2 (CH₂BrOOClO) → TS2 → IM3 (CH₂BrOClO₂) process is 16.3 kcal mol⁻¹. In any case, the isomerization of IM2 → TS2 → IM3 is energetically more favorable than the isomerization of IM1 → TS1 → IM2 by 11.9 kcal mol⁻¹. Therefore, once IM2 (CH₂BrOOClO) is formed, IM1 can easily convert to IM3. At the CCSD(T)//B3LYP level, the energy of IM1 (CH₂BrOOOCl), IM2 (CH₂BrOOClO) and IM3 (CH₂BrOClO₂) are −17.1, 2.2 and −8.0 kcal mol⁻¹ relative to CH₂BrO₂ + ClO, respectively, which may involve various dissociation processes, and will be discussed below.

**3.1.2 Decomposition channels from IM1 (CH₂BrOOOCl) on the singlet PES.** The energy-rich addition complex IM1 (CH₂BrOOOCl) could decompose to various products. Through TS3, with the 1,4-H shift and the breaking of the O–O bond of the nearly planar HCOOO ring, associated with the breakage of the isolated O–Cl bond (pointed out of the plane), the product
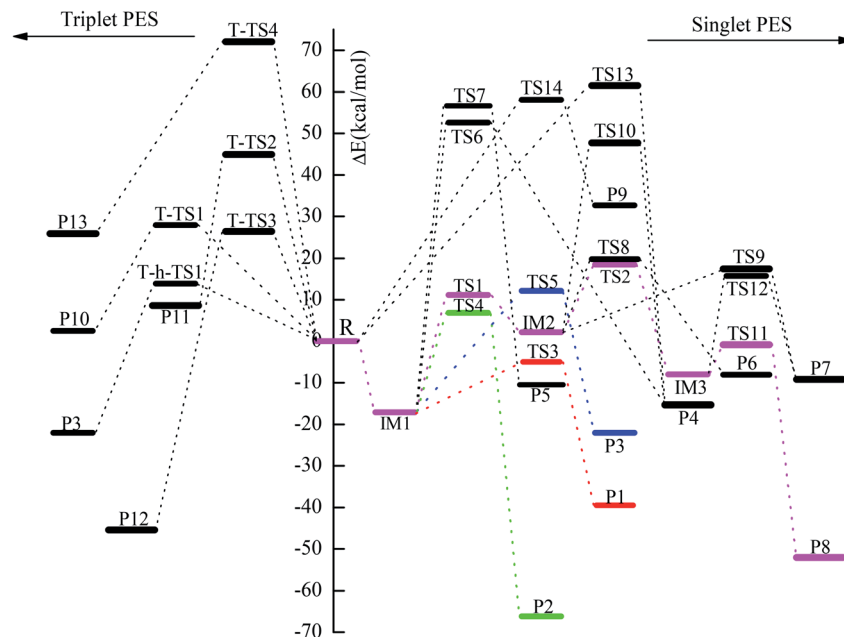
**Fig. 3** Potential energy diagram of the reaction channels for the reaction of $CH_2BrO_2$ with ClO at the CCSD(T)/cc-pVTZ//B3LYP/6-311++G(d,p) level.

P1 (CHBrO + $HO_2$ + Cl) is formed, which is the most feasible pathway in energy. The barrier for the IM1 → TS3 → P1 process is 12.1 kcal $mol^{-1}$. The elimination channel is the most exothermic ($\Delta H = 32.9$ kcal $mol^{-1}$), and the relative Gibbs free energy ($\Delta G$) is $-47.5$ kcal $mol^{-1}$ (Table S1†), indicating that the decomposition pathway to P1 (CHBrO + $HO_2$ + Cl) is spontaneous and contributes more to the reaction under certain conditions.

The second route involves the HOOCl-elimination through TS4, with one of the hydrogen atoms in the $-CH_2Br$ group moving to the middle-O atom of the $-OOO-$ skeleton. The breaking C–H and O–O bonds in the HCOO four-center structure TS4 are stretched to 1.179 and 2.128 Å, and the forming O–H bond is 1.704 Å long. Although the whole R ($CH_2BrO_2$ + ClO) → IM1 ($CH_2BrOOOCl$) → TS4 → P2 (HOOCl + CHBrO) reaction is highly exothermic by about 60.6 kcal $mol^{-1}$, and the relative Gibbs free energy ($\Delta G$) is $-66.7$ kcal $mol^{-1}$ (Table S1†), the barrier for the IM1 → TS4 → P2 process is 24.0 kcal $mol^{-1}$, indicating that this HOOCl-elimination process is spontaneous and may be efficient in the high temperature region.

The production of the P3 ($CHBrO_2$ + HOCl) channel from IM1 ($CH_2BrOOOCl$) takes place via an HCOOO five-centered-ring. As shown in Fig. 1, TS5 occurs via the migration of one of the hydrogen atoms in the $-CH_2Br$ group to the middle-O atom of the $-OOCl$ skeleton accompanied by cleavage of the O–O bond. In the five-center HCOOO structure, the length of the H atom to either the C atom or the O atom is 1.167 or 1.546 Å, respectively, and the broken O–O bond is 2.562 Å. The IM1 ($CH_2BrOOOCl$) → TS5 → P3 ($CHBrO_2$ + HOCl) reaction is moderately exothermic by 16.4 kcal $mol^{-1}$, and the HOCl-elimination barrier is predicted to be 29.2 kcal $mol^{-1}$, which are 17.1 and 5.2 kcal $mol^{-1}$ higher than the processes of IM1 →

TS3 → P1 and IM1 → TS4 → P2, respectively, suggesting that the HOCl-elimination pathway is less competitive with the production of the P1 (CHBrO + $HO_2$ + Cl) and P2 (HOOCl + CHBrO) pathways, and may be unimportant for the $CH_2BrO_2$ + ClO reaction.

In addition, the –ClO group or Cl atom shifting from IM1 ($CH_2BrOOOCl$) respectively undergoes the COOO four-center transition state TS6 or COOOCl five-center transition state TS7 to produce P4 ($CH_2BrOCl + O_2(^1\Delta_g)$) and P5 ($CH_2BrCl + O_3$). In TS6, the C–O and O–O bonds that will be broken and the C–O bond that will be formed are extremely long at 2.619, 1.831, and 2.440 Å, respectively. In TS7, the breaking C–O and O–Cl bonds and the forming C–Cl bond are 2.429, 2.326, and 2.804 Å, respectively. The vibrational frequency analysis of TS6 and TS7 suggest only one imaginary frequency of 378i and 461i $cm^{-1}$, respectively. The energy barriers for the dissociation of IM1 ($CH_2BrOOOCl$) → TS6 → P4 ($CH_2BrOCl + O_2 (^1\Delta_g)$) and IM1 ($CH_2BrOOOCl$) → TS7 → P5 ($CH_2BrCl + O_3$) are extremely high, 69.7 and 73.7 kcal $mol^{-1}$, respectively, and thus these two dissociation channels may be excluded judging from the higher barrier heights.

**3.1.3 Decomposition channels from IM2 ($CH_2BrOOClO$) on the singlet PES.** When we considered the decomposition channels from IM2 ($CH_2BrOOClO$), it could undergo respective O–O bond breaking associated with the 1,4-Br shift or 1,5-Br shift from the C to the Cl atom or the terminal-O atom of the –OClO skeleton (i.e., TS8 and TS9) to yield the final product P6 ($CH_2O + BrClO_2$) and P7 ($CH_2O + BrOClO$). In TS8 and TS9, the loose COOClBr five-membered ring and COOClOBr six-membered ring are non-planar, respectively. In TS8, the Cl–Br bond that will be formed and the C–Br and O–O bonds that will be broken are as long as 3.252, 2.407, and 2.081 Å, respectively.

In TS9, the breaking O–O and C–Br bonds and the forming Br–O bond are 2.096, 2.272, and 2.944 Å, respectively. The barrier heights for the channels of IM2 (CH$_2$BrOOClO) → TS8 → P6 (CH$_2$O + BrClO$_2$) and IM2 (CH$_2$BrOOClO) → TS9 → P7 (CH$_2$O + BrOClO) are 17.6 and 15.2 kcal mol$^{-1}$, which are 1.3 kcal mol$^{-1}$ higher and 1.1 kcal mol$^{-1}$ lower than the process of IM2 → TS2 → IM3, suggesting that these three channels could be competitive with each other.

P4 (CH$_2$BrOCl + O$_2$($^1\Delta_g$)) could also be produced from IM2 (CH$_2$BrOOClO) *via* transition state TS10 involving the terminal-O atom migrating to the carbon atom, associated with the C–O and Cl–O bonds breaking. The located loose COOClO five-centered-ring is non-planar in TS10. In comparison with the production channels of P6 (CH$_2$O + BrClO$_2$) and P7 (CH$_2$O + BrOClO) from IM2 (CH$_2$BrOOClO), the pathway of IM2 (CH$_2$BrOOClO) → TS10 → P4 (CH$_2$BrOCl + O$_2$) has a higher dissociation barrier (45.6 kcal mol$^{-1}$), meaning this decomposition pathway may not be plausible for the title reaction.

### 3.1.4 Decomposition channels from IM3 (CH$_2$BrOClO$_2$) on the singlet PES.

Two possible decomposition channels from IM3 (CH$_2$BrOClO$_2$) are the elimination of the HOClO or BrOClO to form CHBrO or CH$_2$O, respective with either the H atom or Br atom in the –CH$_2$Br group shifting to the O atom, associated with the O–Cl bond cleavage. The BrOClO-elimination is not important compared with the HOClO-eliminations, as the BrOClO-elimination barrier is 16.6 kcal mol$^{-1}$ higher than the HOClO-elimination. Moreover, the overall exothermicity of the IM3 → TS11 → P8 (CHBrO + HOClO) and IM3 → TS12 → P7 (CH$_2$O + BrOClO) reactions are 46.3 and 3.0 kcal mol$^{-1}$, implying that P8 (CHBrO + HOClO) is easily produced once IM3 (CH$_2$BrOClO$_2$) is produced.

### 3.1.5 S$_N$2 displacement channels on the singlet PES.

The O atom or the Cl atom in the ClO radical could attack the C site of CH$_2$BrO$_2$, kicking off the O$_2$ ($^1\Delta_g$) and producing the CH$_2$BrOCl or CH$_2$BrClO, respectively. The transition states involved in these two substitution steps are TS13 and TS14, respectively. The forming and breaking C–O bond in TS13 are 2.050 and 1.794 Å, meanwhile the forming C–Cl bond and breaking C–O bond in TS14 are 2.811 and 2.224 Å, respectively. The barrier heights for these two channels, 61.5 and 58.1 kcal mol$^{-1}$, are rather high, therefore, these two elementary substitution channels are prohibited for the title reaction.

## 3.2 The mechanisms on the triplet PES

H-abstraction and S$_N$2 displacement reaction mechanisms are presented on the triplet surface. The P3 (CHBrO$_2$ + HOCl) products on the triplet PES, exothermic by 16.4 kcal mol$^{-1}$, can be achieved by the O atom of the ClO radical directly abstracting from the –CH$_2$Br group through T-h-TS1. The barrier of CH$_2$BrO$_2$ + ClO → T-h-TS1 → P3 (CHBrO$_2$ + HOCl) is 13.9 kcal mol$^{-1}$, which involves the lowest barrier on the PES. Four S$_N$2 displacement reaction channels between CH$_2$BrO$_2$ and ClO could take place on the triplet PES. The Cl atom of the ClO radical could attack the carbon atom or the terminal oxygen atom of the CH$_2$BrO$_2$, kicking off the O$_2$ ($^3\Sigma$) or CH$_2$BrO to give CH$_2$BrClO or OClO *via* T-TS1 or T-TS2, or the oxygen

atom of the ClO radical could attack the carbon atom or the middle oxygen atom of the CH$_2$BrO$_2$, simultaneously with the departure of O$_2$($^3\Sigma$) and O($^3$P), leading to CH$_2$BrOCl or CH$_2$BrOOCl *via* T-TS3 or T-TS4, respectively. The predicted heat of reaction for the production of P10 (CH$_2$BrClO + O$_2$($^3\Sigma$)), P11 (CH$_2$BrO + OClO), P12 (CH$_2$BrOCl + O$_2$($^3\Sigma$)) and P13 (CH$_2$BrOOCl + O($^3$P)) is 8.5, 14.1, −39.6 and 31.7 kcal mol$^{-1}$, respectively. The above four substituent channels involve high barriers (28.0, 45.0, 26.4 and 72.0 kcal mol$^{-1}$) with respect to the reactants, which are 14.1, 31.1, 12.5 and 58.1 kcal mol$^{-1}$ higher than that of the H-abstraction pathway, thus, these four substituent routes on the triplet are not competitive with the H-abstraction pathway.

## 3.3 Rate constant calculations

As discussed above, for the reaction pathways producing P1, P2, P3, P6, P7 and P8 (Scheme 1), the reaction energy barriers are lower and the reactions are exothermic, so these reaction pathways are involved in the kinetics calculations. However, the reaction pathways producing P4, P5, P9, P10, P11, P12 and P13 with higher energy barriers are less competitive in energy, and their contribution to the total reaction is negligible.

Temperature- or pressure-dependent rate constants for the important pathways (Scheme 2) of the CH$_2$BrO$_2$ + ClO reaction were calculated at 200–3000 K and 10$^{-10}$ to 10$^{10}$ atm using RRKM theory, based on the optimized geometries, moment of inertia and frequencies obtained at the B3LYP/6-311++G(d,p) level, and the energies were obtained at the CCSD(T)/cc-pVTZ level.

The steady-state approximation for all energized intermediates (IM1*, IM2* and IM3*) leads to the following expressions:

$$k_{IM1}(T,P) = \frac{\alpha_a}{h} \frac{Q_t^{\neq} Q_r^{\neq}}{Q_{CH_2BrO_2} Q_{ClO}} e^{-E_a/RT}$$
$$\times \int_0^\infty \frac{\omega}{X_3} N_a(E^{\neq}) e^{-E^{\neq}/RT} dE^{\neq} \quad (1)$$

$$k_{IM2}(T,P) = \frac{\alpha_a}{h} \frac{Q_t^{\neq} Q_r^{\neq}}{Q_{CH_2BrO_2} Q_{ClO}} e^{-E_a/RT}$$
$$\times \int_0^\infty \frac{\omega X_2}{X_3} N_a(E^{\neq}) e^{-E^{\neq}/RT} dE^{\neq} \quad (2)$$

$$k_{IM3}(T,P) = \frac{\alpha_a}{h} \frac{Q_t^{\neq} Q_r^{\neq}}{Q_{CH_2BrO_2} Q_{ClO}} e^{-E_a/RT}$$
$$\times \int_0^\infty \frac{\omega X_1 X_2}{X_3} N_a(E^{\neq}) e^{-E^{\neq}/RT} dE^{\neq} \quad (3)$$

$$k_{P1}(T,P) = \frac{\alpha_a}{h} \frac{Q_t^{\neq} Q_r^{\neq}}{Q_{CH_2BrO_2} Q_{ClO}} e^{-E_a/RT}$$
$$\times \int_0^\infty \frac{k_2(E)}{X_3} N_a(E^{\neq}) e^{-E^{\neq}/RT} dE^{\neq} \quad (4)$$

$$k_{P2}(T,P) = \frac{\alpha_a}{h} \frac{Q_t^{\neq} Q_r^{\neq}}{Q_{CH_2BrO_2} Q_{ClO}} e^{-E_a/RT}$$
$$\times \int_0^\infty \frac{k_3(E)}{X_3} N_a(E^{\neq}) e^{-E^{\neq}/RT} dE^{\neq} \quad (5)$$

$$CH_2BrO_2 + ClO \underset{1}{\overset{a}{\rightleftharpoons}} IM1 \xrightarrow[\text{(TS3)}]{2} P1 \; (CHBrO + HO_2 + Cl)$$

$$\xrightarrow[\text{(TS4)}]{3} P2 \; (CHBrO + HOOCl)$$

$$\xrightarrow[\text{(TS5)}]{4} P3 \; (CHBrO_2 + HOCl)$$

$$\underset{6 \; \text{(TS1)}}{\overset{5}{\rightleftharpoons}} IM2 \xrightarrow[\text{(TS8)}]{7} P6 \; (CH_2O + BrClO_2)$$

$$\xrightarrow[\text{(TS9)}]{8} P7 \; (CH_2O + BrOClO)$$

$$\underset{10 \; \text{(TS2)}}{\overset{9}{\rightleftharpoons}} IM3 \xrightarrow[\text{(TS11)}]{11} P8 \; (CHBrO + HOClO)$$

$$CH_2BrO_2 + ClO \xrightarrow{\text{(T-h-TS1)}} P3 \; (CHBrO_2 + HOCl)$$

$$IMj* \xrightarrow{\omega} IMj$$
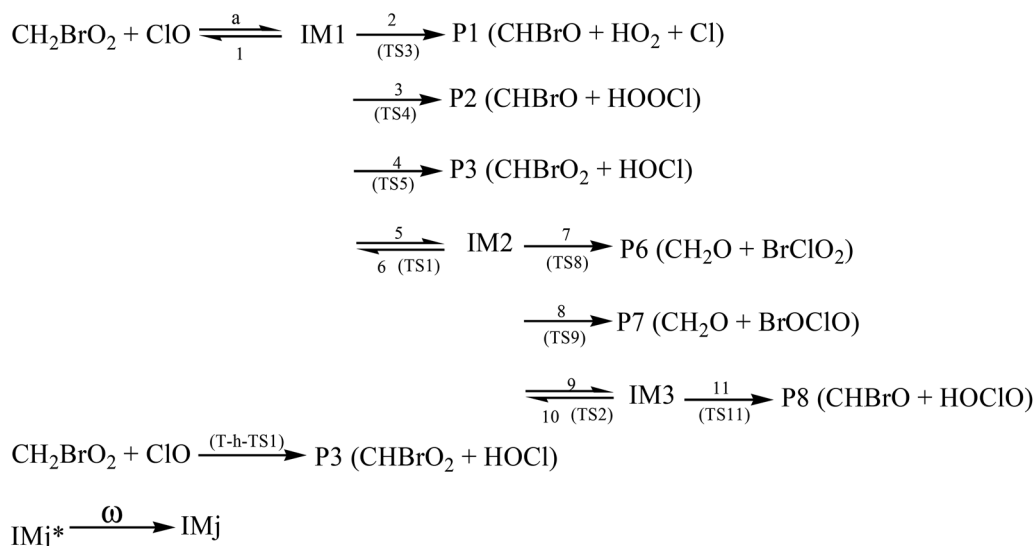
**Scheme 2** The dominant channels for the $CH_2BrO_2 + ClO$ reaction.

$$k_{P3}(T,P) = \frac{\alpha_a}{h} \frac{Q_t^{\neq} Q_r^{\neq}}{Q_{CH_2BrO_2} Q_{ClO}} e^{-E_a/RT}$$
$$\times \int_0^\infty \frac{k_4(E)}{X_3} N_a(E^{\neq}) e^{-E^{\neq}/RT} dE^{\neq} \quad (6)$$

$$k_{P6}(T,P) = \frac{\alpha_a}{h} \frac{Q_t^{\neq} Q_r^{\neq}}{Q_{CH_2BrO_2} Q_{ClO}} e^{-E_a/RT}$$
$$\times \int_0^\infty \frac{k_7(E)X_2}{X_3} N_a(E^{\neq}) e^{-E^{\neq}/RT} dE^{\neq} \quad (7)$$

$$k_{P7}(T,P) = \frac{\alpha_a}{h} \frac{Q_t^{\neq} Q_r^{\neq}}{Q_{CH_2BrO_2} Q_{ClO}} e^{-E_a/RT}$$
$$\times \int_0^\infty \frac{k_8(E)X_2}{X_3} N_a(E^{\neq}) e^{-E^{\neq}/RT} dE^{\neq} \quad (8)$$

$$k_{P8}(T,P) = \frac{\alpha_a}{h} \frac{Q_t^{\neq} Q_r^{\neq}}{Q_{CH_2BrO_2} Q_{ClO}} e^{-E_a/RT}$$
$$\times \int_0^\infty \frac{k_{11}(E)X_1X_2}{X_3} N_a(E^{\neq}) e^{-E^{\neq}/RT} dE^{\neq} \quad (9)$$

with the following definitions:

$$X_1 = k_9(E)/(k_{10}(E) + k_{11}(E) + \omega)$$

$$X_2 = k_5(E)/(k_6(E) + k_7(E) + k_8(E) + k_9(E) + \omega - k_{10}(E)X_1)$$

$$X_3 = k_1(E) + k_2(E) + k_3(E) + k_4(E) + k_5(E) + \omega - k_6(E)X_2$$

In the above equations, $\alpha_a$ is the statistical factor for the reaction path a, and $E_a$ is the energy barrier for the reaction step a. $Q_{ClO}$ and $Q_{CH_2BrO_2}$ are the total partition functions of ClO and $CH_2BrO_2$, respectively; $Q_t^{\neq}$ and $Q_r^{\neq}$ are the translational and rotational partition functions of the entrance transition state, respectively; $N_a(E^{\neq})$ is the number of states for the association transition state with excess energy $E^{\neq}$ above the association

barrier. $k_i(E)$ is the energy-specific rate constant for the $i$th channel and $C_i$ is the ratio of the overall rotational partition function of the TS$_i$ and IM$_j$.

Based on the above thermodynamic results obtained at the CCSD(T)//B3LYP level, the kinetic calculations were performed for the dominant addition/elimination channels (on the singlet PES) and the direct H-abstraction channel (on the triplet PES) using RRKM theory. The temperature dependence of the total and individual rate constants at a selected temperature range of 200–3000 K are shown in Fig. 4. The rate constants for IM1 ($CH_2BrOOOCl$), IM2 ($CH_2BrOOClO$), IM3 ($CH_2BrOClO_2$), P1 ($CHBrO + HO_2 + Cl$), P2 ($CHBrO + HOOCl$), P3 ($CHBrO_2 + HOCl$), P6 ($CH_2O + BrClO_2$), P7 ($CH_2O + BrOClO$), and P8 ($CHBrO + HOClO$) and the rate constants of the H-abstraction channel on the triplet PES are labeled as $k_{IM1}$, $k_{IM2}$, $k_{IM3}$, $k_{P1}$, $k_{P2}$, $k_{P3}$, $k_{P6}$, $k_{P7}$, $k_{P8}$ and $k_{T-h-TS1}$, respectively. The overall rate constant for the $CH_2BrO_2 + ClO$ reaction is denoted as $k_{over}$, where $k_{over} = k_{IM1} + k_{IM2} + k_{IM3} + k_{P1} + k_{P2} + k_{P3} + k_{P6} + k_{P7} + k_{P8} + k_{T-h-TS1}$.

Fig. 4 reveals the contributions of IM1, IM2, IM3, P1, P2, P3, P6, P7, P8 and the H-abstraction channel on the triplet PES to the $CH_2BrO + ClO$ reaction *versus* 1000/T between 200 and 3000 K. Fig. 4 indicates that $k_{IM1}$ reveals weak temperature dependence at $T \leq 600$ K first and then decreases with increasing temperature, and the rate constants for other pathways exhibit a positive temperature dependence at 200–3000 K. The contribution of IM1 ($CH_2BrOOOCl$) takes over the reaction below 600 K. Meanwhile, the contribution of P1 ($CHBrO + HO_2 + Cl$) becomes more important than that of other products at $T > 600$ K. For example, the values of $k_{IM1}/k_{over}$ are 1.00 at 200 K and 0.62 at 600 K (Fig. 5), respectively. However, as the temperature increases, the channel of production of P1 ($CHBrO + HO_2 + Cl$) overcomes IM1 ($CH_2BrOOOCl$) and becomes predominant, and the ratios of $k_{P1}/k_{over}$ are 0.56 at 600 K, 0.94 at 1400 K and 0.66 at 3000 K (Fig. 5).

RRKM calculated the overall high-pressure limit rate constants $k_{inf(over)}$ and the individual high-pressure limit rate
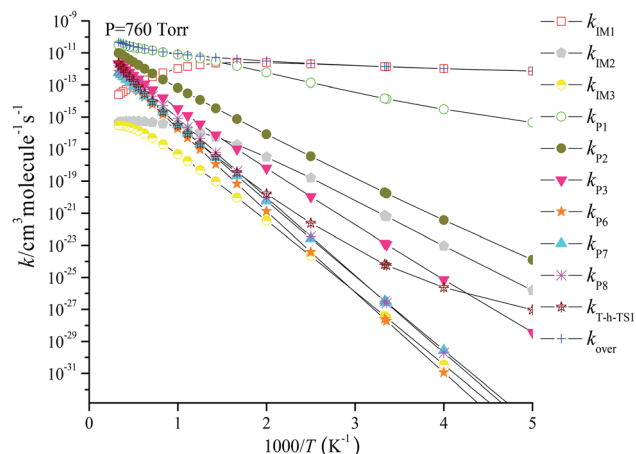
**Fig. 4** Predicted rate coefficients of total and individual primary pathways at 760 torr, $N_2$ in the temperature region of 200–3000 K for the $CH_2BrO_2$ + ClO reaction.



**Fig. 6** Predicted high-pressure limit rate coefficients of total and individual primary pathways at high pressure in the temperature region of 200–3000 K.

constants $k_{inf(IM1)}$, $k_{inf(IM2)}$, $k_{inf(IM3)}$, $k_{inf(P1)}$, $k_{inf(P2)}$, $k_{inf(P3)}$, $k_{inf(P6)}$, $k_{inf(P7)}$, $k_{inf(P8)}$ and $k_{inf(T-h-TS1)}$ in the temperature range of 200–3000 K are illustrated in Fig. 6. $k_{inf(IM1)}$ is equal to $k_{inf(over)}$, which implies that the most favorable channel is the stabilization of IM1 ($CH_2BrOOOCl$) at 200–3000 K. For the main emphasis is on atmospheric applications, the three-parameter Arrhenius fits the total high-pressure limit rate constants $k_{inf(over)}$ (in units of $cm^3$ per molecule per s) within 200–3000 K as follows:

$$k_{inf(over)} = 2.20 \times 10^{-16} T^{1.54} \exp(-0.54/T)(200 \leq T \leq 3000 \text{ K})$$

We also investigated the pressure effect of the total and branching reaction rate constants at selected temperatures of 298, 500, 1000 and 3000 K (Fig. 7) and a pressure range of $10^{-10}$ to $10^{10}$ torr. Obviously, the overall rate constants are not subject to pressure. At 298, 500, 1000 and 3000 K, the stabilization of the IM1 ($CH_2BrOOOCl$) is the significant channel at $P \geq 10^1$, $P \geq 10^2$, $P \geq 10^4$ and $P \geq 10^6$ torr, respectively; at lower pressure, the
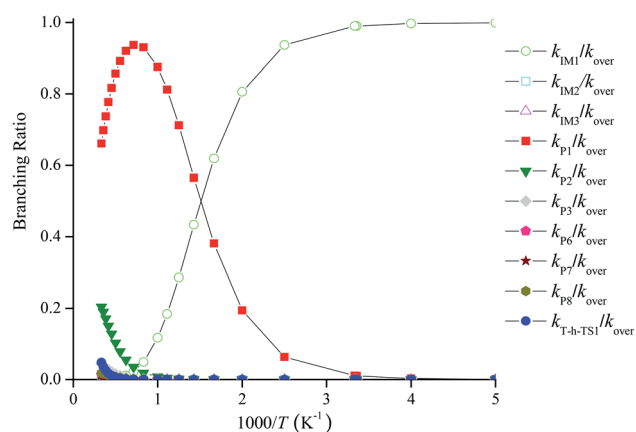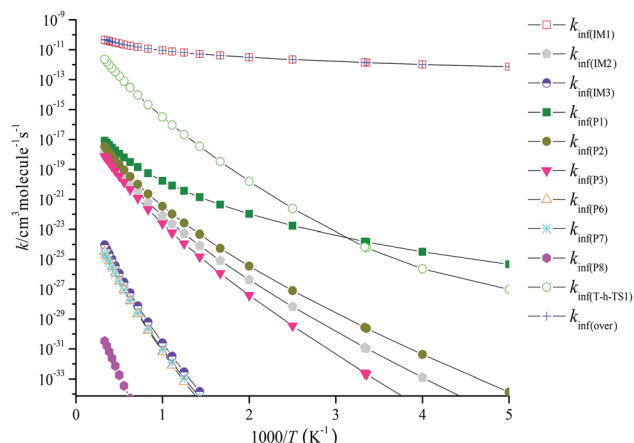
production of P1 (CHBrO + $HO_2$ + Cl) is the dominant reaction channel.

### 3.4 Vertical excitation energy of IM1 ($CH_2BrOOOCl$), IM2 ($CH_2BrOOClO$) and IM3 ($CH_2BrOClO_2$)

The photo-oxidation of compounds containing bromine and chlorine is significant for Br and Cl atmospheric chemistry, which as sources of Br and Cl, the photolysis might affect the stratosphere and troposphere. To gain new insights into the photolytic stability of the Br and Cl containing compounds, the vertical excitation energy ($T_V$) of the first ten excited states for IM1 ($CH_2BrOOOCl$), IM2 ($CH_2BrOOClO$) and IM3 ($CH_2BrOClO_2$) were calculated by the TDDFT method using B3LYP/6-311++G(d,p), and the results comprising wavelength ($\lambda$), excitation energy ($T_V$) and oscillator strength ($f$) are listed in Table 1. Compounds will be considered to photolyze if the $T_V$ value is smaller than 4.1 eV or the wavelength is longer than 300 nm.[39,40] From Table 1, it is seen that the $T_V$ value of the first three excited states of IM1 ($CH_2BrOOOCl$) and IM3 ($CH_2BrOClO_2$) are 382 nm (3.2 eV), 340 nm (3.6 eV), and 329 nm (3.7 eV) and 482 nm (2.5 eV), 465 nm (2.6 eV), and 410 nm (3.0 eV), respectively, and their oscillator strengths are 0.0014, 0.0003, and 0.0168, and 0.0021, 0.0202, and 0.0035. The first four excited states of IM2 ($CH_2BrOOClO$) are 684 nm (1.8 eV), 374 nm (3.3 eV), 364 nm (3.4 eV) and 331 nm (3.7 eV), and the oscillator strengths are 0.0001, 0.0082, 0.0075, and 0.0041, respectively, indicating the possibility of photolysis of IM1 ($CH_2BrOOOCl$), IM2 ($CH_2BrOOClO$) and IM3 ($CH_2BrOClO_2$) under sunlight, which will cause them to be an origin of reactive bromine and chlorine species in the atmosphere.

### 3.5 Atmospheric lifetime of $CH_2BrO_2$

The atmospheric lifetime of $CH_2BrO_2$ can be calculated using the following formula: $\tau = \dfrac{1}{k[\text{ClO}]}$. Using the total rate constants, $1.37 \times 10^{-12}$ $cm^3$ per molecule per s for the $CH_2BrO_2$ + ClO reaction at 298 K and the global atmospheric ClO



**Fig. 5** Forecasted branching ratios for the $CH_2BrO_2$ + ClO reaction at 760 torr.
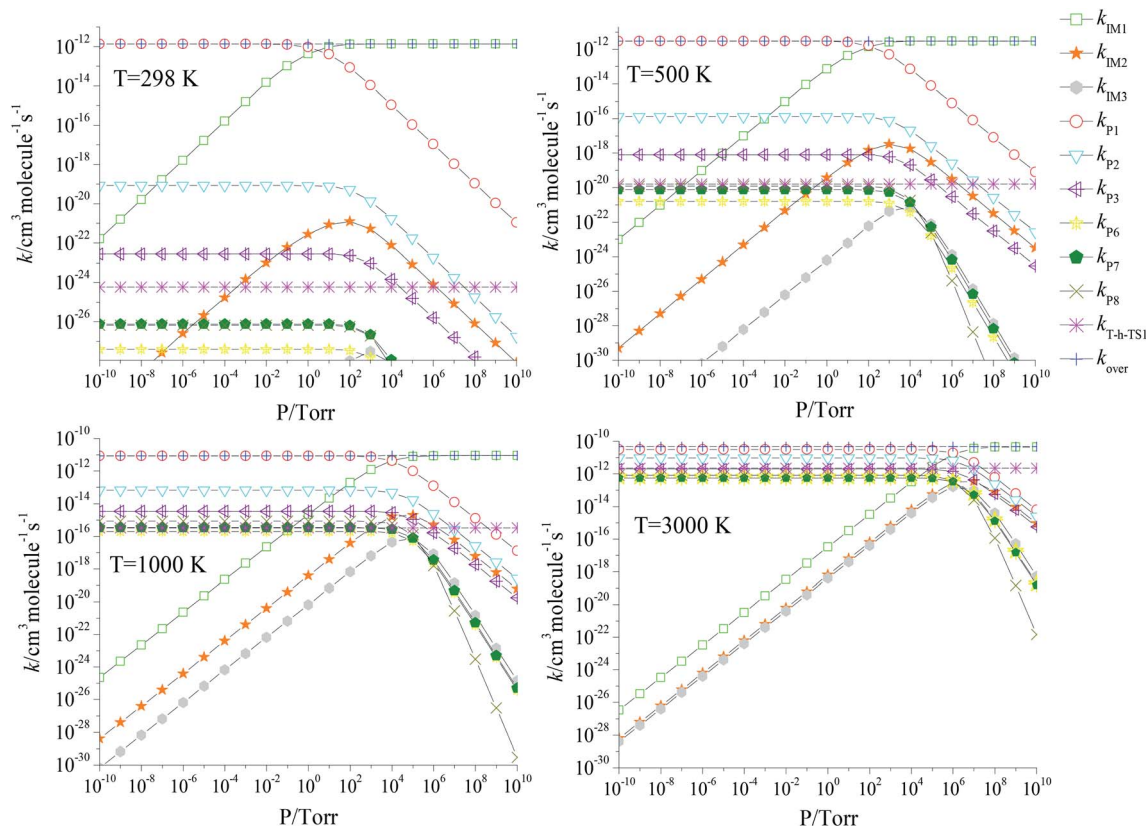
**Fig. 7** Predicted rate coefficients of total and individual primary pathways at high pressures in the temperature region of 200–3000 K.

concentrations $1 \times 10^7$ molecules per cm$^3$,[41] the lifetime of $CH_2BrO_2$ was estimated to be 20.27 h, which suggests that the reaction of $CH_2BrO_2$ + ClO plays an important role in some special areas and the marine boundary layer.

### 3.6 Atmospheric implications of CHBrO

With the concentration of around $10^7$ molecules per cm$^3$ in the stratosphere, OH/ClO radicals play a significant role in the degradation processes of many molecules.[42] Thus, the formation of CHBrO as a major product in the title reaction could lead

to further reactions with OH and ClO, respectively. To be thorough, the CHBrO + ClO/OH reactions were studied by the same methods, and the corresponding PESs are depicted in Fig. 8a and b, as well. According to the calculations, two channels were located *via* different transition states for these two reactions. The first scenario starts from transition states TS-ClO or TS-OH surmounting the barrier of 16.55 or 8.00 kcal mol$^{-1}$, leading to the final products HCOOCl + Br or HCOOH + Br, respectively. Moreover, the hydrogen atom in CHBrO could be abstracted by OH/ClO radicals *via* h-TS-ClO or h-TS-OH. The IRC calculation

**Table 1** The excitation energy $T_V$ (in eV), oscillator strength $f$ (in atomic units) and wavelength $\lambda$ (in nm) of the first five excited states of IM1 (CH$_2$BrOOOCl), IM2 (CH$_2$BrO$_2$ClO) and IM3 (CH$_2$BrOClO$_2$) at the TD-B3LYP/6-311++(d,p) level of theory

| Excited states | IM1 (CH$_2$BrOOOCl) | | | IM2 (CH$_2$BrOOClO) | | | IM3 (CH$_2$BrOClO$_2$) | | |
|---|---|---|---|---|---|---|---|---|---|
| | $T_V$ | $F$ | $\lambda$ | $T_V$ | $f$ | $\lambda$ | $T_V$ | $f$ | $\lambda$ |
| 1 | 3.2 | 0.0014 | 382.37 | 1.8 | 0.0001 | 684.81 | 2.5 | 0.0021 | 482.56 |
| 2 | 3.6 | 0.0003 | 340.18 | 3.3 | 0.0082 | 374.45 | 2.6 | 0.0202 | 465.33 |
| 3 | 3.7 | 0.0168 | 329.99 | 3.4 | 0.0075 | 364.59 | 3.0 | 0.0035 | 410.05 |
| 4 | 4.2 | 0.0003 | 294.26 | 3.7 | 0.0041 | 331.18 | 4.1 | 0.0518 | 299.90 |
| 5 | 4.4 | 0.0095 | 277.97 | 4.2 | 0.1482 | 289.55 | 4.3 | 0.0018 | 286.12 |
| 6 | 5.1 | 0.0037 | 239.07 | 4.8 | 0.0014 | 253.87 | 5.4 | 0.2292 | 229.05 |
| 7 | 5.2 | 0.0199 | 234.54 | 5.4 | 0.0297 | 226.09 | 5.4 | 0.0293 | 226.33 |
| 8 | 5.45 | 0.0592 | 227.54 | 5.6 | 0.0049 | 217.93 | 5.6 | 0.0007 | 219.90 |
| 9 | 5.6 | 0.0084 | 220.97 | 5.8 | 0.0002 | 211.35 | 5.8 | 0.0018 | 212.98 |
| 10 | 5.6 | 0.0882 | 218.85 | 6.1 | 0.0077 | 202.31 | 5.9 | 0.0013 | 206.78 |

confirms that the corresponding product is BrCO + HOCl or BrCO + $H_2O$. The barrier height of h-TS-ClO and h-TS-OH is about 25.46 and $-1.36$ kcal mol$^{-1}$. Thus, the OH-initiated reaction might be one of the main removal pathways for CHBrO.

### 3.7 Comparisons with the similar reaction of $CH_3O_2$ + ClO

In order to gain a deeper understanding of the reaction of $CH_2BrO_2$ + ClO, it is very important to compare the mechanism and kinetics between the title reaction and a similar system ($CH_3O_2$ + ClO).[43] It is concluded that the addition/elimination and $S_N2$ displacement mechanisms are found both on the singlet PES of the above two reactions. On the triplet PES, H-abstraction and $S_N2$ displacement mechanisms are found for the $CH_2BrO_2$ + ClO reaction and only addition/elimination is identified for the $CH_3O_2$ + ClO reaction. By comparing the two reactions, we find that the most favorable channel is the oxygen atom in ClO attacking the terminal-O atom in $CH_2BrO_2$ and $CH_3O_2$, forming the intermediate $CH_2BrOOOCl$ and $CH_3$-OOOCl, and then decomposition to the final products CHBrO + $HO_2$ + Cl and $CH_2O$ + HOOCl. The Br-substituted effect could be speculated to be of no significant role in the reactions of

$CH_2BrO_2$ and $CH_3O_2$ with ClO in the atmospheric conditions. Also, no kinetic behaviors were discovered for the $CH_3O_2$ + ClO reaction theoretically. The total rate constants show temperature dependence and pressure independence for the reaction between $CH_2BrO_2$ and ClO.

## 4.　Conclusions

The atmospheric oxidation process of $CH_2BrO$ + ClO was studied at the CCSD(T)//B3LYP level of theory. H-abstraction and $S_N2$ displacement mechanisms on the triplet PES, and addition/elimination and $S_N2$ displacement mechanisms on the singlet PES were identified, respectively. The dominant reaction mechanism on the triplet PES is H-abstraction, and on the singlet PES, addition/elimination. The rate constants of the title reaction at 200–3000 K have been calculated employing a Fortran code based on RRKM theory. According to the obtained kinetics data, the ClO-addition to the terminal-O of $CH_2BrO_2$ producing IM1 ($CH_2BrOOOCl$) dominates the title reactions at $T \geq 600$ K on the singlet PES, and the O atom of ClO abstracting one of the H atoms in $CH_2BrO_2$ dominates the whole reaction at $T > 600$ K on the triplet PES. The atmospheric lifetime of $CH_2BrO_2$ in the presence of ClO is predicted to be 20.27 h. IM1 ($CH_2BrOOOCl$), IM2 ($CH_2BrOOClO$) and IM3 ($CH_2BrOClO_2$) will photolyze under sunlight, which might be one source of Br and Cl containing species in the atmosphere.

## Conflicts of interest

There are no conflicts to declare.

## Acknowledgements

## References

1　B. Finlayson-Pitts and J. N. Pitts Jr, *Chemistry of the Upper and Lower Atmosphere*, Academic Press, New York, 1999.

2　R. P. Wayne, *Chemistry of Atmospheres*, Oxford University Press, Oxford, 3rd edn, 2000.

3　D. L. Albritton and R. T. Watson, *Methyl Bromide: Its Atmospheric Science, Technology and Economics, Montreal Protocol Assessment Supplement*. UNEP, Nairobi, Kenya, 1993.

4　S. A. Montzka and S. Reimann, *et al.*, Ozone-depleting substances (ODSs) and related chemicals. Scientific Assessment of Ozone Depletion: 2010, *Global Ozone Research and Monitoring Project Report No. 52*, World Meteorological Organization, Geneva, Switzerland, ch. 1, 2011.

5　W. S. McGivern, H. Kim, J. S. Francisco and S. W. North, *J. Phys. Chem. A*, 2004, **108**, 7247–7252.

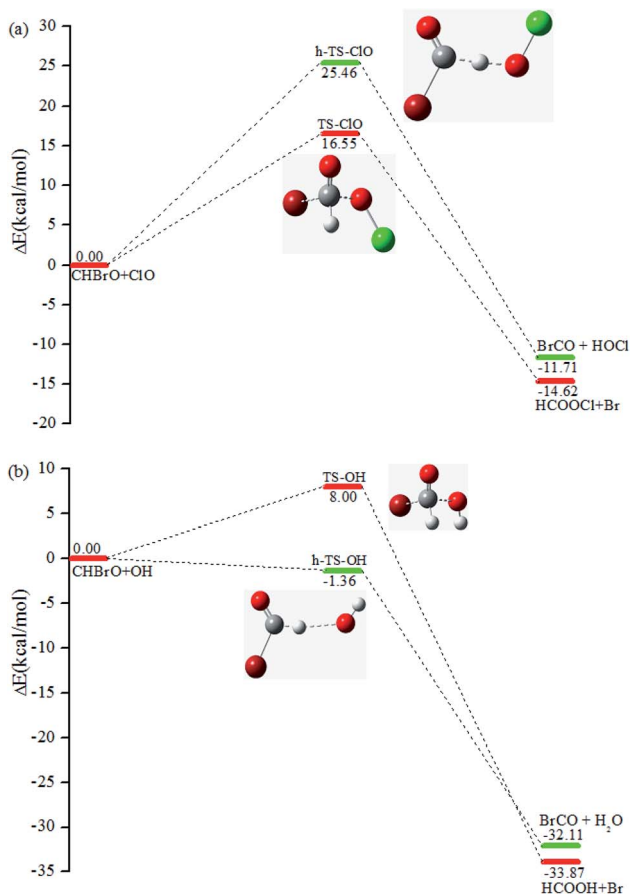6　K. M. Hickson, L. F. Keyser and S. P. Sander, *J. Phys. Chem. A*, 2007, **111**, 8126–8138.

**Fig. 8** Reaction channels and relative energy (unit: kcal mol$^{-1}$) at the CCSD(T)/cc-pVTZ//B3LYP/6-311++G(d,p) level. (a) The energetic profile of the CHBrO with ClO reaction. (b) The energetic profile of the CHBrO with OH reaction.

**RSC Advances**  Paper

7 S. L. Nickolaisen, S. M. Roehl, L. K. Blakely, R. R. Fridel, J. S. Francisco, R. F. Liu and S. P. Sander, *J. Phys. Chem. A*, 2000, **104**, 308–319.

8 G. P. Knight, T. Beiderhase, F. Helleis, G. K. Moortgat and J. N. Crowley, *J. Phys. Chem. A*, 2000, **104**, 1674–1685.

9 Z. F. Xu, R. S. Zhu and M. C. Lin, *J. Phys. Chem. A*, 2003, **107**, 3841–3850.

10 E. Drougas, A. F. Jalbout and A. M. Kosmas, *J. Phys. Chem. A*, 2003, **107**, 11386–11390.

11 F. Helleis, J. N. Crowley and G. K. Moortgat, *J. Phys. Chem.*, 1993, **97**, 11464–11473.

12 F. Helleis, J. N. Crowley and G. K. Moortgat, *Geophys. Res. Lett.*, 1994, **21**, 1795–1798.

13 A. S. Kukui, T. P. W. Jungkamp and R. N. Schindler, *Ber. Bunsen Phys Chem.*, 1994, **98**, 1298–1302.

14 Y. Z. Tang, H. F. Sun, J. Y. Sun, Y. J. Zhang and R. S. Wang, *Atmos. Environ.*, 2014, **92**, 367–375.

15 A. Horowitz, G. Schuster and G. K. Moortgat, *Int. J. Chem. Kinet.*, 1992, **24**, 255–269.

16 F. X. Wu and R. W. Carr, *J. Phys. Chem.*, 1995, **99**, 3128–3136.

17 K. A. Holbrook, M. J. Pilling and S. H. Robertson, *Unimolecular Reactions*, J. Wiley, Chichester, UK, 1996.

18 H. Hou, B. S. Wang and Y. S. Gu, *J. Phys. Chem. A*, 2000, **104**, 320–328.

19 H. Hou and B. S. Wang, *J. Chem. Phys.*, 2007, **127**, 054306.

20 J. A. Manion and I. A. Awan, *Int. J. Chem. Kinet.*, 2018, **50**, 225–242.

21 Y. Z. Tang, C. G. Lu, J. Y. Sun, *et al*, *Environ. Sci. Pollut. Res.*, 2019, **26**, 2345–2352.

22 S. H. Mousavipour, S. Ramazani and Z. Shahkolahi, *J. Phys. Chem. A*, 2009, **113**, 2838.

23 Y. J. Zhang, J. Y. Sun, W. Q. Zhang, Y. Z. Tang and R. S. Wang, *J. Comput. Chem.*, 2014, **35**, 1646–1656.

24 A. D. Becke, *J. Chem. Phys.*, 1993, **98**, 5648.

25 C. Lee, W. Yang and R. G. Parr, *Phys. Rev. B*, 1988, **37**, 785.

26 J. Zhao and R. Y. Zhang, *Atmos. Environ.*, 2008, **42**, 5849–5858.

27 Y. Z. Tang and C. J. Nielsen, *Atmos. Environ.*, 2012, **55**, 185–189.

28 C. Gonzalez and H. B. Schlegel, *J. Chem. Phys.*, 1989, **90**, 2154–2161.

29 C. Gonzalez and H. B. Schlegel, *J. Phys. Chem.*, 1990, **94**, 5523–5527.

30 K. Raghavachari, G. W. Trucks, J. A. Pople and M. Head-Gordon, *Chem. Phys. Lett.*, 1989, **157**, 479–483.

31 T. J. Lee and P. R. Taylor, *Int. J. Quantum Chem.*, 1989, **23**, 199.

32 J. Peiró-García and I. Nebot-Gil, *ChemPhysChem*, 2003, **4**, 843.

33 J. Peiró-García and I. Nebot-Gil, *J. Comput. Chem.*, 2003, **24**, 1657.

34 J. C. Rienstra-Kiracofe, W. D. Allen and H. F. Schaefer X, *J. Phys. Chem. A*, 2000, **104**, 9823.

35 M. J. Frisch, G. W. Trucks, H. B. Schlegel, G. E. Scuseria, M. A. Robb, J. R. Cheeseman, G. Scalmani, V. Barone, B. Mennucci, G. A. Petersson, H. Nakatsuji, M. Caricato, X. Li, H. P. Hratchian, A. F. Izmaylov, J. Bloino, G. Zheng, J. L. Sonnenberg, M. Hada, M. Ehara, K. Toyota, R. Fukuda, J. Hasegawa, M. Ishida, T. Nakajima, Y. Honda, O. Kitao, H. Nakai, T. Vreven, J. A. Montgomery Jr, J. E. Peralta, F. Ogliaro, M. Bearpark, J. J. Heyd, E. Brothers, K. N. Kudin, V. N. Staroverov, R. Kobayashi, J. Normand, K. Raghavachari, A. Rendell, J. C. Burant, S. S. Iyengar, J. Tomasi, M. Cossi, N. Rega, J. M. Millam, M. Klene, J. E. Knox, J. B. Cross, V. Bakken, C. Adamo, J. Jaramillo, R. Gomperts, R. E. Stratmann, O. Yazyev, A. J. Austin, R. Cammi, C. Pomelli, J. W. Ochterski, R. L. Martin, K. Morokuma, V. G. Zakrzewski, G. A. Voth, P. Salvador, J. J. Dannenberg, S. Dapprich, A. D. Daniels, O. Farkas, J. B. Foresman, J. V. Ortiz, J. Cioslowski, D. J. Fox, Gaussian, Inc, Wallingford CT, 2009.

36 S. E. Stein and B. S. Rabinovitch, *J. Chem. Phys.*, 1973, **58**, 2438–2445.

37 D. C. Astholz, J. Troe and W. Wieters, *J. Chem. Phys.*, 1979, **70**, 5107–5116.

38 NIST Computational Chemistry Comparison and Benchmark Database, http://srdata.nist.gov/cccbdb/.

39 Y. Z. Tang, H. F. Sun, J. Zhao, J. H. Liu and R. S. Wang, *Atmos. Environ.*, 2013, **65**, 164–170.

40 Y. Z. Tang, H. F. Sun, J. Y. Sun, Y. J. Zhang and R. S. Wang, *Atmos. Environ.*, 2014, **92**, 367–375.

41 C. T. Chang, T. H. Liu and F. T. Jeng, *Environ. Res.*, 2004, **94**, 67–74.

42 J. G. Anderson, *Geophys. Res. Lett.*, 1976, **3**, 165–168.

43 A. M. Kosmas and E. Drougas, *Chem. Phys.*, 2009, **358**, 230–234.